^{92}Mo$(n,xn\,yp\,z\,\alpha\,\gamma)$ reactions for neutron energies up to 250 MeV

P. E. Garrett, L. A. Bernstein, J. A. Becker, K. Hauschild,* C. A. McGrath,† D. P. McNabb, and W. Younes
Lawrence Livermore National Laboratory, Livermore, California 94551

M. B. Chadwick, G. D. Johns, R. O. Nelson, and W. S. Wilburn
Los Alamos National Laboratory, Los Alamos, New Mexico 87545

E. Tavukcu
North Carolina State University, Raleigh, North Carolina 27695

S. W. Yates
University of Kentucky, Lexington, Kentucky 40506-0055
(Received 14 June 2000; published 10 October 2000)

Excitation functions from the interaction of fast neutrons (up to an energy of 250 MeV) on a target of ^{92}Mo have been measured. Yields have been determined for reaction γ rays from $^{88-92}$Mo, $^{88-92}$Nb, $^{86-91}$Zr, $^{84-86,88}$Y, and $^{80,82-86}$Sr. These results are compared with model calculations using the GNASH code which takes into account compound nucleus, preequilibrium emission, multiple preequilibrium emission, and direct reaction contributions. The model calculations are in good agreement overall, but significant discrepancies emerge for some high-multiplicity, charged-particle-exit channels.

PACS number(s): 24.10.−i, 24.60.Dr, 25.40.−h, 25.40.Fq

I. INTRODUCTION

The ability to perform neutron cross-section measurements over a wide range of neutron energies up to several hundred MeV provides a unique opportunity to test sophisticated reaction-modeling codes. Cross-section measurements using fast neutrons have been reported typically over a narrow energy range (generally <20 MeV) or at a single energy (usually 14 MeV) and, therefore, there is a serious lack of data on reaction cross sections for higher-energy neutrons. In the energy range up to several hundred MeV, a region is entered where preequilibrium (or precompound) reactions are the dominating reaction mechanism in the early stages of the reaction; this regime has not been well explored with neutron-induced reactions. There is both a lack of data and a lack of comparisons with model predictions.

With the advent of the GEANIE (germanium array for neutron induced excitations) spectrometer [1] at the Los Alamos Neutron Science Center (LANSCE), a large scale γ-ray detection array has been coupled to a spallation neutron source for the first time. One main goal of the GEANIE project was to measure absolute γ-ray production cross sections from neutron-induced reactions, and thus the array has been optimized for this purpose. The measured absolute detection efficiency for the array, combined with a well-characterized sample, allows the determination of partial γ-ray cross sections. The use of spallation neutrons produced by a pulsed proton beam has the advantage that cross sections as a function of the neutron energy (excitation functions) can be determined by employing the time-of-flight method. The parent nuclei for the prompt γ rays emitted from the reaction can be identified using knowledge of the level schemes and from the energy thresholds for the γ rays determined from the experiment.

In a previous experiment with a target of ^{196}Pt [2], $(n,15n)$ reactions were observed, but no evidence of charged-particle emission was obtained. A target of ^{92}Mo was chosen for the present study to probe how neutron-deficient nuclei in this mass region were populated in neutron-induced reactions, including charged-particle-exit channels. Because the Zr region is rich with isomeric states, it was also of interest to observe γ rays populating the isomeric and ground states since the isomer to ground-state population ratio has a number of practical applications. Another goal was to investigate the competition between α-particle emission and the corresponding $2p2n$ process. Excitation functions for γ rays originating from 26 different isotopes were obtained; for 14 of these isotopes, there is strong evidence for composite-particle emission. Also, excitation functions for γ rays populating both the ground state and isomeric states were extracted for several isotopes.

The observation of 26 different isotopes in the present work provides a demanding test of reaction model calculations, and is the first study in this mass region to extract γ-ray excitation functions for so many different reaction channels over the range of neutron bombarding energies up to $E_n=250$ MeV. The results of the present work were compared with calculations performed with the computer program GNASH [3], which employs Hauser-Feshbach calculations with preequilibrium and direct reaction contributions. One advantage of GNASH calculations over some other reaction codes is the ability to calculate partial γ-ray cross sections. This is particularly important when the final channel product is in an odd or odd-odd nucleus for which the γ-ray cascade can be severely fragmented. One sensitivity of the

*Present address: DAPNIA/SPhN CEA Saclay, Bat 703 l'Orme des Merisiers, F-91191 Gif-sur-Yvette, France.

†Present address: Idaho National Engineering and Environmental Laboratory, P.O. Box 1625, Idaho Falls, ID 83415.

calculations, however, is that they are dependent on the accuracy of the level schemes. In some cases, incomplete knowledge of the level scheme, such as missed strong feeding transitions, incorrect branching ratios, etc., introduces a bias into the calculations. While this generally is not a problem for even-even, or most odd, nuclei in the region of ^{92}Mo, it does raise a cautionary note regarding comparisons with nuclei that have not been thoroughly investigated by a variety of means. Model predictions with a Hauser-Feshbach code such as GNASH are therefore challenging since, for good agreement with experiment, theory must correctly predict the overall break-up channel cross sections and in addition correctly predict the angular momentum transfers and γ-ray cascades in the residual nuclei. As will be discussed in greater detail below, the main results from the present study are (1) overall, the calculations reproduce the data well, in most cases within 50%, and (2) the main problems appear to be associated with the treatment of the γ-ray cascade.

In Sec. II, the details of the experiments are given. The GNASH calculations are outlined in Sec. III and are compared with the experimental excitation functions in Sec. IV. The main results of this study are summarized in Sec. V.

II. EXPERIMENTAL DETAILS

Measurements were performed at the LANSCE Weapons Neutron Research (WNR) facility. Spallation neutrons are produced by bombarding a ^{nat}W target with 800 MeV protons from the LANSCE linac. The pulsed proton beam was delivered with a 1.8 μs spacing for 625 μs macropulses at a macropulse rate of typically 80 Hz resulting in a duty factor of 5%. The ''white'' neutron spectrum thus produced has a maximum energy near 800 MeV, although for energies above $\sim$8 MeV the neutron flux decreases rapidly with the conditions used in this experiment. The scattering sample consisted of 13 g of metallic Mo powder, enriched to 99% in ^{92}Mo, located at a distance of 20.34 m from the production target on the 60R flight path at LANSCE-WNR. The neutrons were collimated to produce a 2 cm diameter beam spot at this location. In order to reduce the number of low-energy neutrons and the intensity of γ rays from the neutron production target, approximately 7.5 cm of polyethylene and 2.9 cm of Pb were placed in the neutron beam 14 m upstream of the scattering sample. Permanent magnets removed charged particles from the flight line.

The scattering sample was placed at the focus of the GEANIE spectrometer [1], which consisted of 11 planar detectors and 15 25% hpGe coaxial detectors. All planar detectors were equipped with BGO-suppression shields with NaI nose cones, while only 9 of the coaxial detectors were equipped with BGO-suppression shields. The planar detectors were concentrated at the most forward and backward angles and γ-ray events of $\leqslant$1 MeV were processed, while the coaxial detectors were positioned around $90\pm40°$ and γ-ray events were recorded up to 4 MeV. The front faces of the Ge detectors were located approximately 14 cm from the scattering sample. The trigger used for the data acquisition was one unsuppressed Ge event. The data stream consisted of a bit determining whether the event occurred in or out of the macropulse, the time relative to the start of the macropulse (CLOCK, recorded in 100 ns intervals), the energy E_γ and, if in-beam, the time t_γ relative to the proton micropulse for each detector which indicated an event. The neutron flux was monitored using a fission chamber with both ^{235}U and ^{238}U foils [5].

During playback of the data, events were separated according to in-beam (occurred during the macropulse) or out-of-beam (between macropulses). Various two-dimensional matrices were created which included E_γ vs time of flight (TOF) as well as $\gamma\gamma$ coincidences for the in-beam data, and E_γ vs CLOCK and $\gamma\gamma$ coincidences for the out-of-beam data. The collection of data between the macropulses proved to be very advantageous as the spectra were rather rich in γ rays from well-studied β^+ and EC decays. Since the activity was produced by the neutrons, the efficiency curve constructed from the out-of-beam data included the effects of the beam spot geometry and target attenuation and thus could be applied directly to the in-beam data. It was, however, difficult to find uncontaminated calibration lines at the very low and high γ-ray energies; the efficiency curve is, therefore, most reliable between E_γ=140 keV and 3 MeV. Typical uncertainties on the relative efficiency are 3–5 %, and for the strongest γ rays dominate the uncertainty in the cross section. The energy calibration was performed using the energies of well-known lines in ^{92}Mo from the in-beam data and selected β-decay lines, and was ''bootstrapped'' upwards in energy by calculating the energy of a high-energy γ-ray branch from levels in ^{92}Mo where a lower-energy, precisely known γ ray was also issued.

Shown in Fig. 1 is the spectrum obtained with the coaxial Ge detectors after selecting the TOF of the events corresponding to 10–250 MeV neutrons. Those γ rays whose excitations functions are shown in Figs. 2–14 are labeled by their energy and the isotope from which they originate. The top panel of the figure shows in detail the 100–400 keV region, where a number of low-energy γ rays, particularly from the Nb isotopes, yielded unambiguous excitation functions.

The excitation functions were obtained by applying TOF gates 15 ns wide, the typical full width at half maximum for the time resolution for the sum of the coaxial detectors, on the γ-ray events corresponding to neutron energies between 2 and 250 MeV. For each particular γ-ray energy, the time-of-flight was determined by using the prompt γ rays, the γ flash, from the ^{nat}W production target as a time reference. The γ-ray spectra generated by the time gates were fitted and peak areas extracted. Global parameters describing the shapes of the γ-ray peaks as a function of energy were determined, and spectra were fit with the program gf2 [6]. The areas were subsequently divided by the number of neutrons determined to be in the particular energy bin from an analysis of the fission chamber data for both the ^{235}U and ^{238}U foils. A gate on the pulse height above the α-decay events was placed on the fission chamber data, and the events induced by photofission served as the time reference point. Above 20 MeV, the (n,f) cross sections of Lisowski *et al.* [7] were used to convert the number of fissions into a neutron fluence, below 20 MeV the values as compiled in ENDF-VI were used [20].

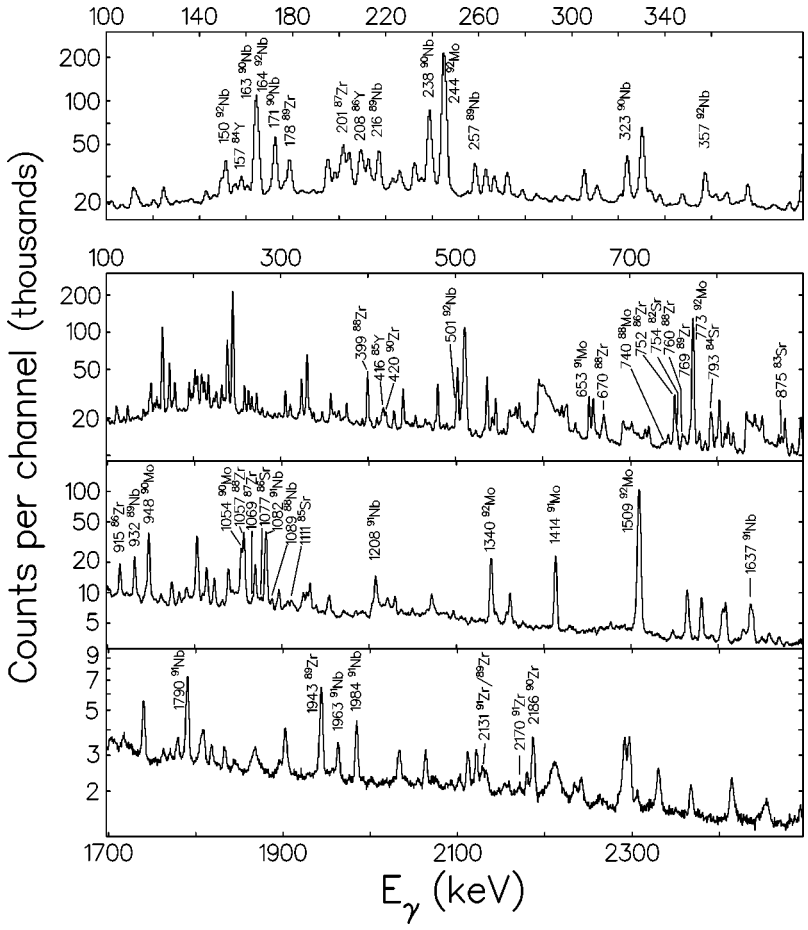

FIG. 1. Spectrum obtained from the sum of the coaxial hpGe detectors for neutron-induced reactions on ^{92}Mo after selecting event times which correspond to neutrons in the energy range of 10 MeV to 250 MeV. Transitions for which excitation functions are displayed in Figs. 3–15 are labeled according to their energies and isotopes of origin.

The ^{92}Mo metallic powder sample consisted of two separate samples of enriched ^{92}Mo material, each mounted in a small latex bag, roughly cylindrical in shape, and suspended in the neutron beam. Since the detailed geometry of this arrangement was unknown, it is not possible to extract absolute cross sections with the present data. Therefore, a one-point normalization was adopted that could be applied to all data, thus allowing a comparison of the relative cross sections with the GNASH calculations. The most appropriate candidate for the normalization was determined to be the 1509-keV $2_1^+ \rightarrow 0_{\text{g.s.}}^+$ transition in ^{92}Mo since the $(n,n'\gamma)$ channel is the strongest reaction channel at low neutron energies and the $2_1^+ \rightarrow 0_{\text{g.s.}}^+$ is expected to represent $\approx$90% of the channel cross section. The shapes of the experimental excitation function for the 1509-keV transition and that from the GNASH calculations, described below, were compared (see Fig. 3), and excellent agreement was found for neutron energies between 5 and 20 MeV. The normalization point corresponding to a neutron bombarding energy of 8 MeV, near the center of the ''plateau'' region of the cross section, was chosen since it was found that at this energy the calculated cross section was relatively stable to minor variations in the input parameters. This one-point normalization was applied to all data. Thus while the overall scale of the cross sections are subject to renormalization the relative scale and the shape are fixed.

Multiple scattering effects in large samples can yield additional apparent cross section at higher neutron energies. This complication arises due to scattering in the sample of a high-energy neutron, for which the particular γ-ray production cross section is low, to a lower energy where the γ-ray production cross section is much higher. Even through only a small fraction of the neutrons undergo multiple scattering, the effect can be significant if the lower-energy cross section is orders of magnitude larger. However, the neutron emission spectrum is weighted towards low-energy neutrons, and thus multiple scattering affects significantly only those reactions which have a low-threshold energy, i.e., in this particular case, the $(n,n'\gamma)$ reaction. A crude estimation obtained by assuming that all the target material is in the beam suggests corrections of $\sim$50% at $E_n = 100$ MeV for the 1509-keV $2_1^+ \rightarrow 0_{\text{g.s.}}^+$ transition in ^{92}Mo. A detailed analysis requires an accurate knowledge of the target geometry; even in cases where the geometry is well known, uncertainties in the correction quickly arise due to its iterative nature and reliance on calculated emission spectra, etc. [4]. Since the target geometry was not well known in the present work, a multiple-scattering correction was not attempted. The excitation functions for the $(n,n'\gamma)$ channel are still deemed reliable up to $E_n \simeq 20$ MeV, since the cross sections are large, but it should be noted that above this energy the omitted multiple-scattering corrections can become increasingly important for the (n,n') channel.

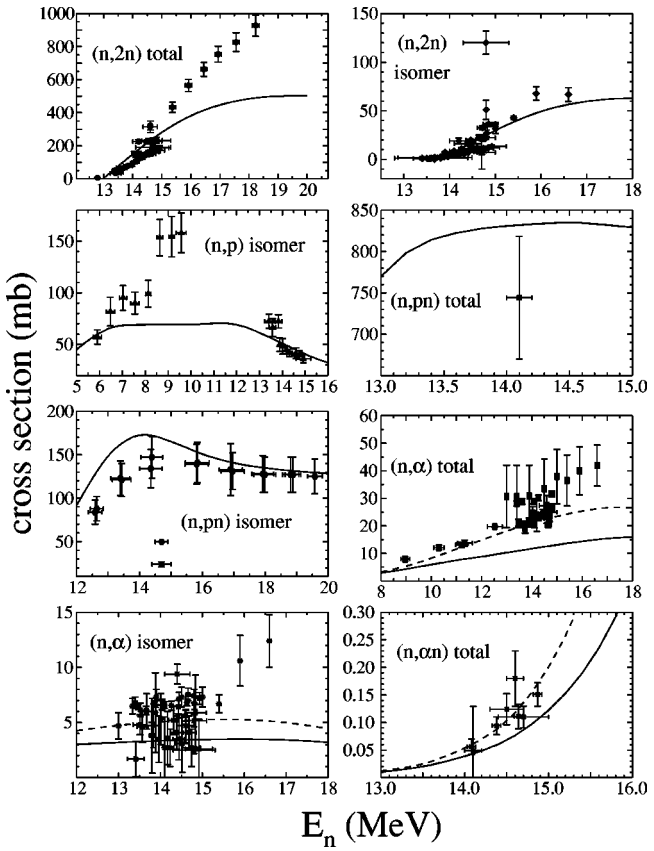

FIG. 2. Total cross sections for the channel, or for the long-lived isomeric state, as indicated compared with the GNASH cross sections. All experimental data are taken from Ref. [20]. There are two distinct trends for the $(n,2n)$ total cross section up to 15 MeV. The GNASH predictions fall between the two trends, and thus underpredict the one data set that extends above 15 MeV. The other reaction channels are reproduced reasonably well, except for the (n,α) data for which the GNASH results using default parameters (solid curve) are approximately a factor of 2 below the measurements.

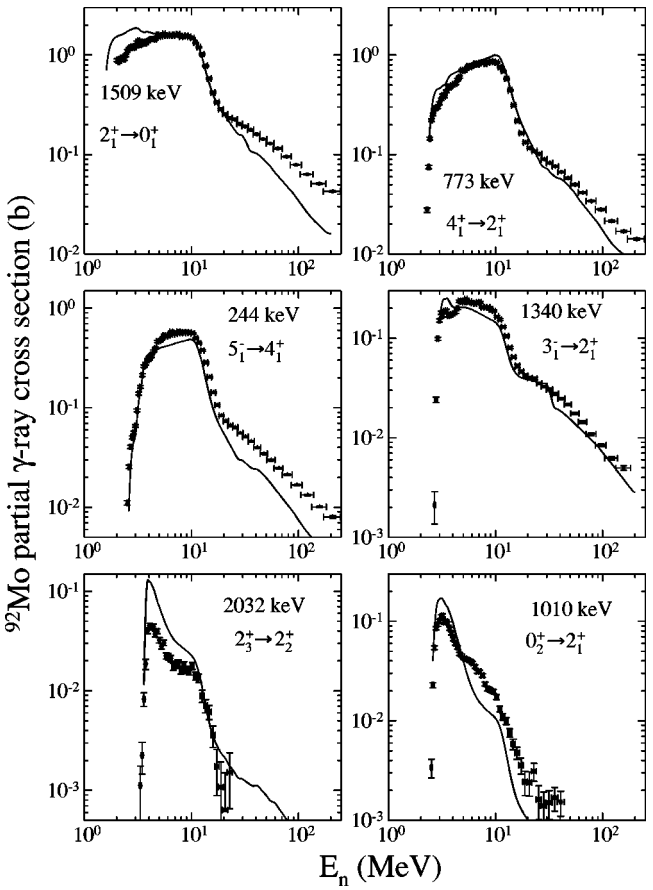

FIG. 3. Excitation functions obtained for γ rays originating from the ^{92}Mo$(n,n'\gamma)$ reaction for neutron energies between 2 and 250 MeV. The transitions are labeled by their energies in keV and their placement in the ^{92}Mo level scheme. The data were normalized to the calculation at 8 MeV neutron energy for the 1509-keV $2_1^+ \rightarrow 0_{\text{g.s.}}^+$ transition. The same normalization factor was applied to all data. The lines show results of GNASH calculations as described in the text.

It should be noted that the uncertainties on the cross sections displayed in the figures and listed in the text include the statistical uncertainties only. Because of the positioning of the coaxial detectors, which provided most of γ-ray data in the present study, there are possible systematic uncertainties from angular distribution effects. Measurements centered about $90° \pm 40°$ will introduce a bias in the γ-ray intensities, mainly from the $a_2 P_2(\cos\theta)$ term in the angular distribution. For quadrupole multipolarities, the yields will be less than the angle-averaged intensity, whereas for dipole transitions the yields will be greater. The error introduced will be larger at threshold (where maximum orientations of the specific levels occur), and decrease rapidly with increasing neutron energy. The effect could be as large as 20% (rarely do a_2 coefficients exceed 0.4) at threshold, and probably do not exceed 10% several MeV above threshold. Therefore, in addition to the systematic uncertainty introduced by the normalization procedure, there could be a $\approx$10% systematic uncertainty arising from angular distribution effects.

III. GNASH CALCULATIONS

Calculations for the γ-ray production cross sections were performed using the GNASH [3] code. The general method of calculation involves assuming that the reaction proceeds in a series of sequential two-body breakup processes. At each stage in the reaction, γ-ray and particle emission can occur and are computed using the Hauser-Feshbach compound nucleus theory which conserves angular momentum and parity. Prior to the composite system reaching an equilibrated state, preequilibrium emission decay probabilities are computed.

Optical model calculations of the total, elastic, and reaction cross sections, and the transmission coefficients for the Hauser-Feshbach calculations, were obtained using the ECIS code [8]. Optical model parameters were taken from global phenomenological models. For neutrons, the Wilmore-Hodgson potential [9] was used below 20 MeV, and at higher energies the medium-energy potential of Madland [10] was employed. For protons, the Perey potential [11] was

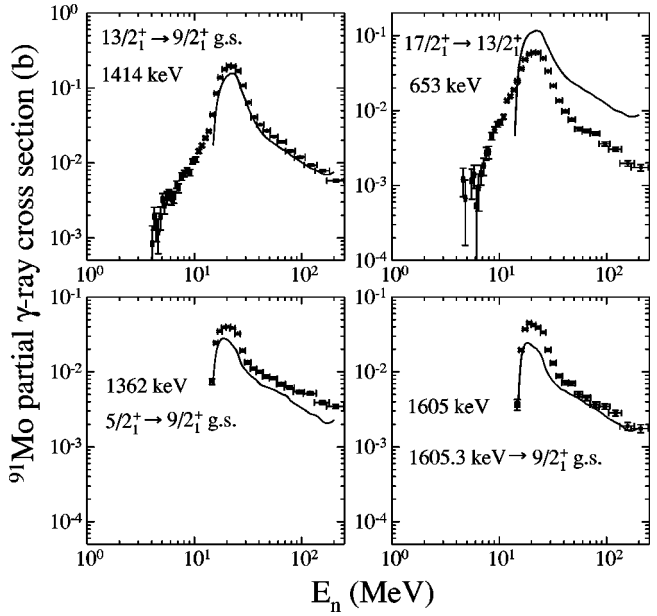

FIG. 4. As for Fig. 3, but for γ rays originating from the ^{92}Mo($n,2n\gamma$)^{91}Mo reaction. The data show clearly the effects of short-lived ($\sim$40 ns) isomers present in this nucleus, which results in apparent cross section below the reaction threshold.

used below 30 MeV, and the Madland medium-energy potential [10] at higher energies. The potential of Lohr [12] was used for deuterons, Becchetti and Greenlees [13] for tritons, and that of McFadden and Satchler [14] for α particles. For γ-ray emission, the strength functions and ''transmission coefficients'' were obtained from the giant-resonance model of Kopecky and Uhl [15]. The excitation-energy dependence of the γ-ray emission is included through the use [15] of generalized Lorentzian forms for the $E1$, $M1$, and $E2$ strength

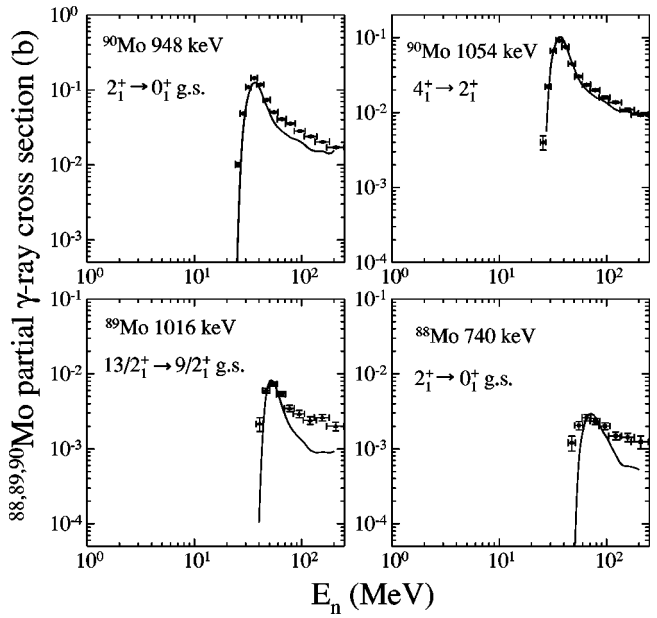

FIG. 5. As for Fig. 3, but for γ rays originating from the ^{92}Mo($n,3n\gamma$)^{90}Mo, ^{92}Mo($n,4n\gamma$)^{89}Mo, and ^{92}Mo($n,5n\gamma$)^{88}Mo reactions.

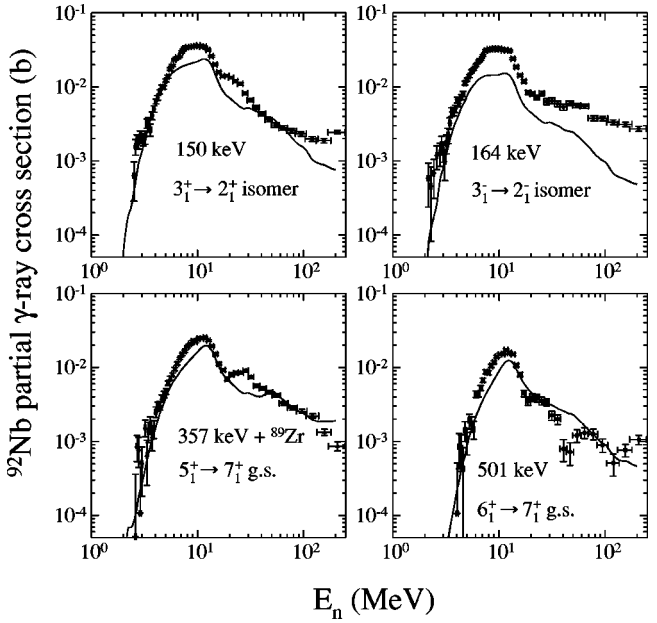

FIG. 6. As for Fig. 3, but for γ rays originating from the ^{92}Mo($n,p\gamma$)^{92}Nb reaction. Excitation functions for transitions into both the 7^+ ground state and the 2^- isomeric state are displayed. The 150-keV and 357-keV transitions appear to have contributions from unresolved γ rays originating from other reactions channels above approximately 15 MeV, resulting in features in the excitation functions not present for the other γ rays shown.

functions, in contrast to the Brink-Axel formalism.

After calculation of the population of the first compound nucleus using the Hauser-Feshbach expressions, corrections for preequilibrium and direct reaction effects are made. The preequilibrium contribution calculations were performed using the exciton model of Kalbach [16] using the code PRECO-B [17]. The one adjustable parameter, the damping matrix element, was taken as 145 MeV^3, based on systematic results obtained from numerous GNASH analyses for reactions at these energies. Multiple preequilibrium emission was included using the model of Ref. [18], and does not include any adjustable parameters. Composite-particle preequilibrium, which includes effects arising from particle pickup, stripping, knockout, etc., are also taken into account using the phenomenology developed by Kalbach [16].

Finally, direct reactions for neutron inelastic scattering were included for scattering to the 2_1^+ and 3_1^- vibrational states in ^{92}Mo using distorted-wave Born approximation theory. The deformation parameters were taken from the compilation given in the International Atomic Energy Agency Reference Input Parameter Library [19], and the neutron optical potential described above.

The most recent information [20] on the level schemes was incorporated, including results from the present experiments which extended the level scheme of ^{92}Mo [21]. The spectroscopic information on the first 15 discrete levels for each nucleus were used, onto which a statistical level density prescription was smoothly mapped. The level density theory of Ignatyuk *et al.* [22] was utilized to model the statistical properties of excited nuclei. This theory is particularly ap-

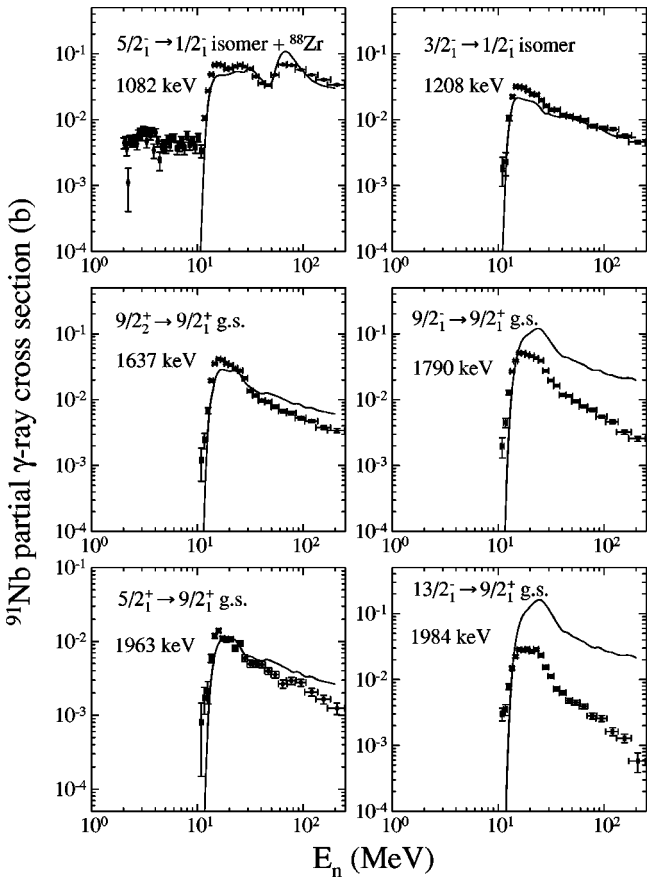

FIG. 7. As for Fig. 3, but for γ rays originating from the ^{92}Mo$(n,pn\gamma)^{91}$Nb reaction. The good agreement for the positive-parity states and poor agreement for the negative-parity states indicates a deficiency in the γ-ray cascade modeling for this nucleus.

propriate for analyses at higher energies since it includes a damping of shell effects in the level density parameter for increasing excitation energies.

IV. DISCUSSION

Including ^{92}Mo, a total of 26 different isotopes were observed for which excitation functions could be extracted, the lightest being ^{80}Sr via the $(n,4p7n)$ channel. The observation of a large number of reaction channels up to $E_n = 250$ MeV provides the most complete set of γ-ray data from neutron-induced reactions in this mass region obtained to date. As such, it provides one of the most demanding tests of reaction model calculations.

The nuclear model calculations have used default input parameters, and indeed this approach was chosen so as to provide an assessment of how well an *a priori* nuclear statistical model calculation can predict γ-ray cross sections. However, in this situation one can expect to see certain deficiencies in the calculations, particularly in small emission channels which are sensitive to nuclear level density parameters which may not be well known. An example of this is discussed in more detail below.

Figure 2 displays the cross sections calculated for channels for which experimental data previously existed [20]. In

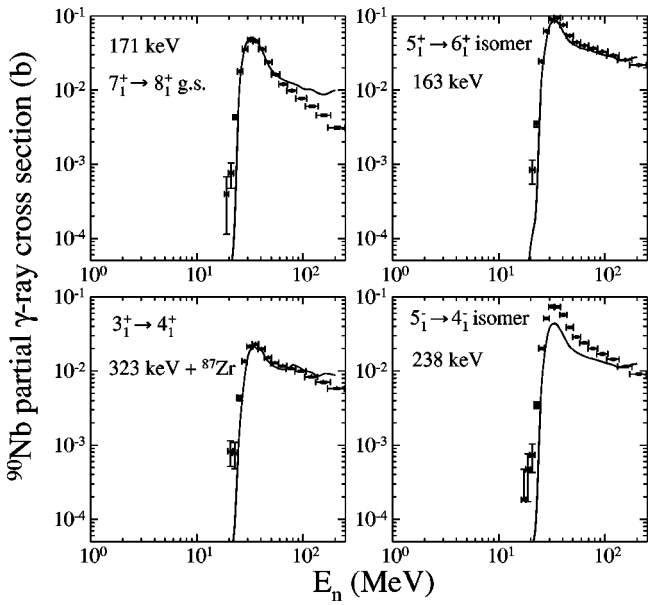

FIG. 8. As for Fig. 3, but for γ rays originating from the ^{92}Mo$(n,p2n\gamma)^{90}$Nb reaction. The deviations between the calculated and observed excitation functions may be related to incomplete knowledge of the level scheme.

^{91}Mo, there are discrepancies between the measurements such that there are two distinct trends in the data; the GNASH results for the channel cross section lie between these two trends. The experimental cross sections for production of the 65 s $I^\pi = \frac{1}{2}^-$ isomer in ^{91}Mo are in good agreement with the GNASH calculations. The (n,p) and (n,pn) channels, as well, display good agreement for the channel cross sections. Therefore, for low neutron bombarding energies, discrepancies in individual γ-ray cross sections cannot be due to poor

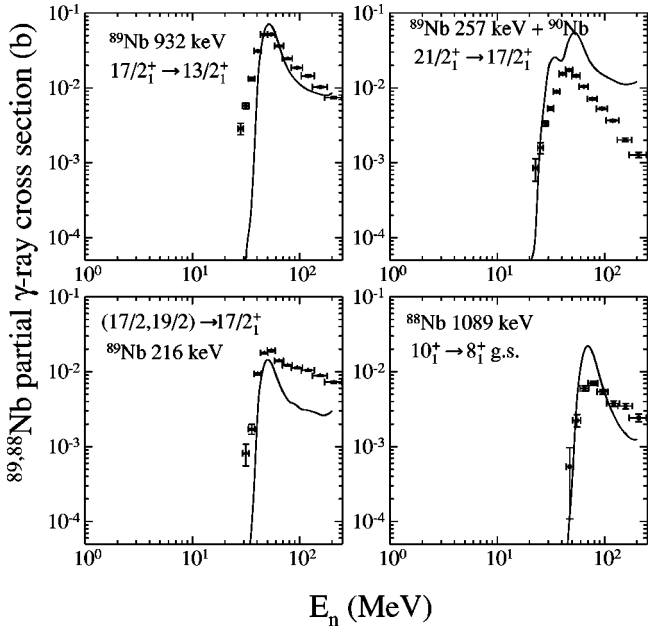

FIG. 9. As for Fig. 3, but for γ rays originating from the ^{92}Mo$(n,p3n\gamma)^{89}$Nb and ^{92}Mo$(n,p4n\gamma)^{88}$Nb reactions.

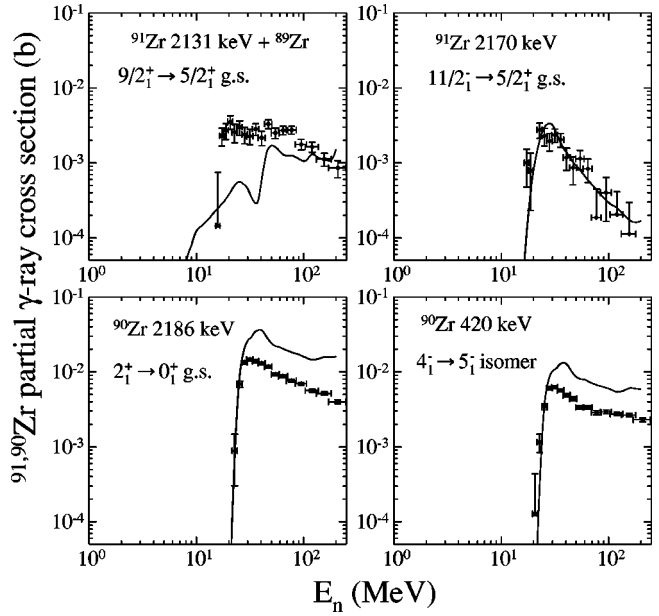

FIG. 10. As for Fig. 3, but for γ rays originating from the ^{92}Mo($n,2p\gamma$)^{91}Zr and ^{92}Mo($n,2pn\gamma$)^{90}Zr reactions. Above $\approx$30 MeV, the excitation function for the 2131-keV transition is contaminated by the presence of an unresolved contribution from an ^{89}Zr.

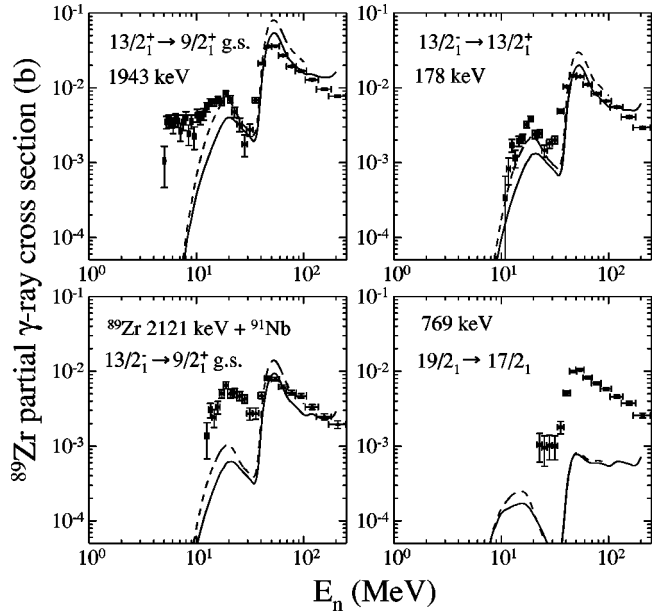

FIG. 11. As for Fig. 3, but for γ rays originating from the ^{92}Mo($n,\alpha/2p2n\gamma$)^{89}Zr reaction. There is a clear distinction between α emission and the $2p2n$ process. The 2121-keV transition is unresolved from a ^{91}Nb γ ray that is believed to contribute less than 10% of the cross section above 30 MeV. The solid curves are results of the GNASH calculations using the default level density parameters whereas the dashed curves are results where the level density parameters for ^{89}Zr have been tuned in an effort to better describe the (n,α) channel.

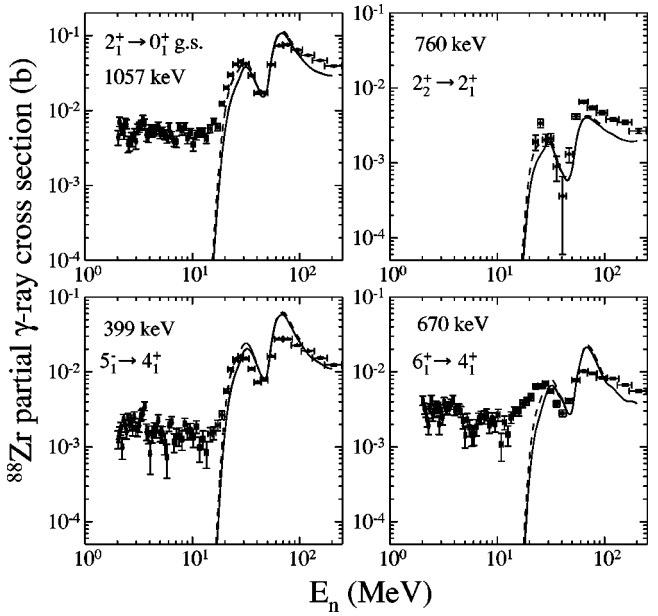

FIG. 12. As for Fig. 3, but for γ rays originating from the ^{92}Mo($n,\alpha n/2p3n\gamma$)^{88}Zr reaction. The effects of long-lived isomers are readily apparent. Note that the peak cross section for the αn-exit channel relative to the $2p3n$-exit channel is greater than the corresponding ratio in ^{89}Zr. The solid curves are results of the GNASH calculations using the default level density parameters whereas the dashed curves are results where the level density parameters for ^{89}Zr have been tuned in an effort to better describe the (n,α) channel.

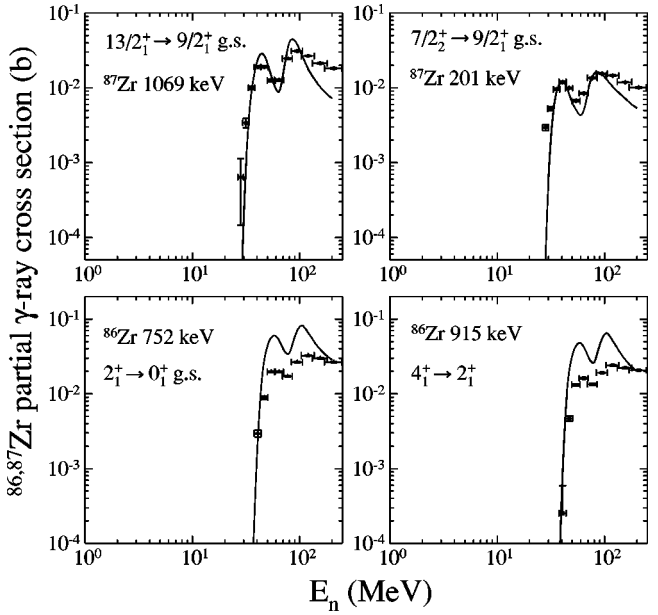

FIG. 13. As for Fig. 3, but for γ rays originating from the ^{92}Mo($n,\alpha 2n/2p4n\gamma$)^{87}Zr and ^{92}Mo($n,\alpha 3n/2p5n\gamma$)^{86}Zr reactions. The observed cross sections for γ rays from ^{86}Zr are a factor of $\approx$3 smaller than calculations predict.

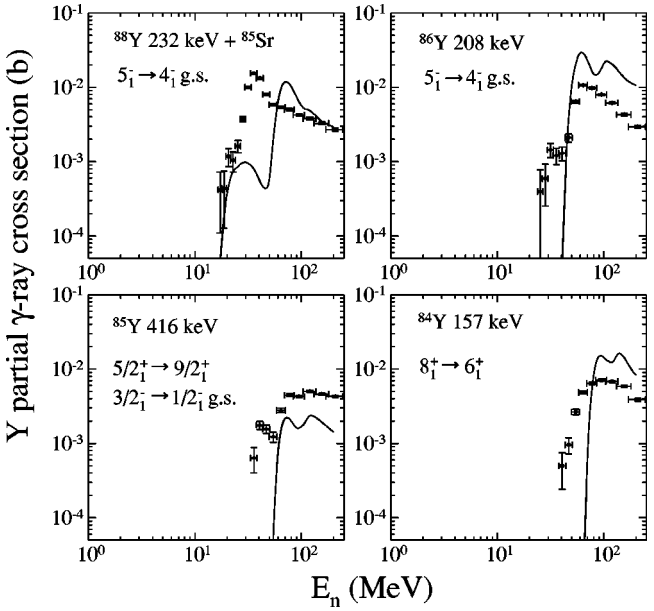

FIG. 14. As for Fig. 3, but for γ rays originating from the Y isotopes ^{88}Y, ^{86}Y, ^{85}Y, and ^{84}Y. In all cases, there is observable cross section below the threshold for the $(n,3pxn)$ reaction channels, at 32.8, 54.2, 63.8, and 75.7 MeV, respectively, implying contributions from the αpxn channel.

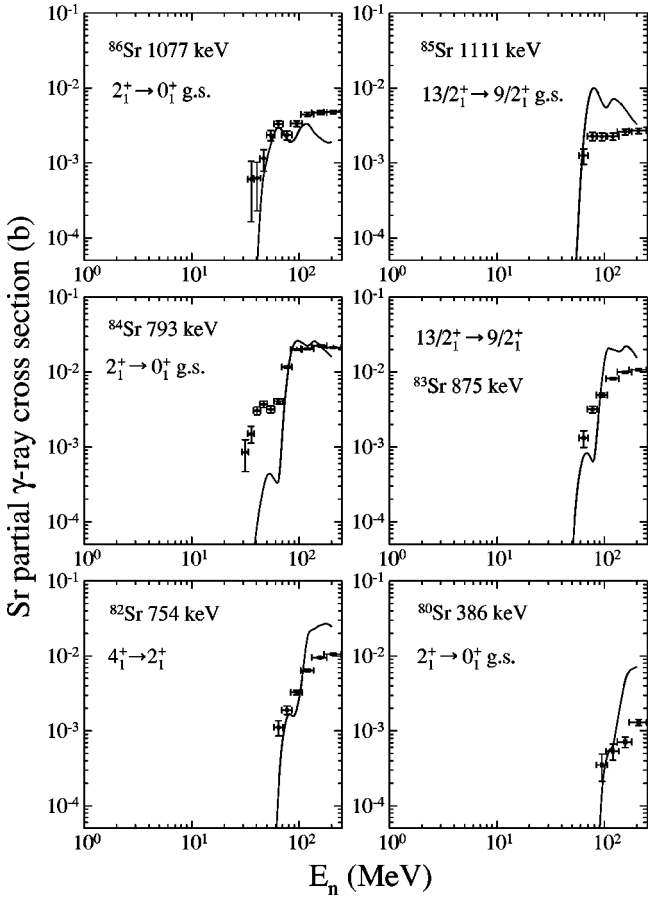

FIG. 15. As for Fig. 3, but for γ rays originating from the Sr isotopes ^{86}Sr, ^{85}Sr, ^{84}Sr, ^{83}Sr, ^{82}Sr, and ^{80}Sr. In all cases, there is observable cross section below the threshold for the $(n,4pxn)$ reaction channels, with thresholds at 48.1, 59.7, 68.3, 80.4, 89.4, and 111.5 MeV, respectively, indicating contributions from the $(n,\alpha 2pxn)$ reactions (with E_{th} at 19.5, 31.1, 39.7, 51.8, 60.7, and 73.4 MeV, respectively). In ^{84}Sr, observable cross section appears below the $(n,\alpha 2p3n)$ threshold, indicating contributions from the $2\alpha n$-exit channel.

reproduction of the channel cross section, but reflect problems in modeling the γ-ray cascade. Overall, the GNASH calculations and the experimental data (examples of excitation functions are shown in Figs. 3–15) agree well over the wide range of neutron bombarding energies, and isotopes, observed in this work. Where problems do arise, they are mostly associated with the modeling of the γ-ray cascade and with multiple charged-particle emission, as will be discussed in the following subsections.

In the case of the (n,α) reaction, the default calculation (solid line in Fig. 2) underpredicts the cross section by about a factor of 2. This emission channel represents a small competition channel to the main neutron (and to a lesser extent, proton) emission channels, representing less than 1% of the cross section at 14 MeV. Therefore, the calculation is particularly sensitive to the nuclear model parameters for this channel, especially the residual nucleus ^{89}Zr level density, and the factor of 2 disagreement between the default calculation and experiment is by no means surprising. Unfortunately, there is no experimental *s*-wave neutron resonance spacing information for the ^{89}Zr system to guide the choice of level density parameters (since ^{88}Zr is not a stable nucleus that can be used as a target for neutron bombardment). Therefore, as a parameter ''tuning'' exercise, the default pairing energy in the level density calculation was decreased by 1.3 MeV in order to improve the agreement with the (n,α) data, which is dominated by compound nucleus α-particle emission, giving the dashed line in Fig. 2. Since the overall (n,α) cross section is now better described, one might expect that the γ rays in this channel from the decay of excited ^{89}Zr nuclei would also be better described. Indeed, in this case the first peak seen in the excitation functions in Fig. 11 corresponding to α emission processes is seen to be better modeled by such calculations (dashed line). However, at higher neutron bombarding energies where the $(n,2p2n)$ reaction dominates the predicted peak partial γ-ray cross sections are typically now a factor of 2 greater than observed. Therefore, the improvement in the predicted cross section for the (n,α) channel comes at the expense of the agreement in the $(n,2p2n)$ channel. The only other reaction channel that displayed significant sensitivity to the tuning of the (n,α) was the $(n,\alpha n)$ channel, results for which are shown in Fig. 12. For neutron bombarding energies from the $(n,\alpha n)$ threshold up to 30 MeV there is a minor improvement in the predicted cross sections, but negligible effect once the $(n,2p3n)$ threshold is crossed. This modification to the calculations does not, though, improve some of the γ rays in other nuclei where discrepancies between theory and experiment were observed, and unfortunately for most nuclei

populated in these reactions there is no experimental level density information to guide the calculations.

A. The Mo isotopes

A total of five Mo isotopes were observed from ^{92}Mo to ^{88}Mo, and Figs. 3–5 display the experimental excitation functions compared with the GNASH calculations. While the overall agreement is rather good, there are some discrepancies worthy of note, particularly at low neutron energies in the (n,n') channel.

1. $^{92}Mo(n,n'\gamma)^{92}Mo$

In ^{92}Mo, the 1509-keV $2_1^+ \rightarrow 0^+_{\text{g.s.}}$ cross section is predicted to rise more rapidly than observed; at 2 MeV the cross section is predicted to be 1.5 b whereas 0.89(3) b is observed. Experimentally the cross section reaches a maximum of 1.5–1.6 b between $E_n = 4.8$ and 8.0 MeV; the calculated maximum occurs at $E_n = 3$ MeV with a value of 1.87 b. However, as noted above, the shape is in excellent agreement between $E_n = 5$ MeV and 20 MeV. Above $E_n = 20$ MeV, the cross section is predicted to fall faster than observed, although much of this may be due to multiple-scattering effects in the data. An examination of the excitation functions for the 4_1^+ and 3_1^- states shows much better agreement for high neutron energies. The 5^- level displays excellent agreement for low neutron energies, up to several MeV above threshold, but shows significant discrepancies at higher neutron energies. Since the 4_1^+ and 5_1^- levels have approximately the same threshold energy (within 300 keV, with the 4_1^+ level being lower), it is probable that not all the discrepancy can be attributed to multiple-scattering effects. The shape at higher neutron energies ($E_n > 20$ MeV) can be contrasted with the behavior of the off-yrast transitions in the bottom panels of the Fig. 3, where very significant differences between the calculated and observed excitation functions occur for neutron energies below 10 MeV. It is clear from Fig. 3 that, in general, the compound cross sections can be overestimated by as much as a factor of 2 for low neutron energies.

2. $^{92}Mo(n,2n\gamma)^{91}Mo$

The results for ^{91}Mo, some of which are shown in Fig. 4, display very good overall agreement between the calculated and observed excitation functions. Of particular note for some of these cases are the effects that isomers have on the observed excitation functions. Since the presence of isomers results in the emission of delayed γ rays, these γ rays are associated with lower neutron energies. Two distinct scenarios arise in the interpretation of the data when isomers are present. In the first scenario, if the γ ray originates from the isomeric level itself or receives a large fraction of its intensity from the decay of an isomer, the net effect is to shift the cross sections curves down in neutron energy and to cause them to be ''smeared'' out. If the isomer is long lived, on the order of several microseconds or longer, the γ ray intensity appears to be independent of the time reference. For short-lived isomers, on the order of a few nanoseconds or less, the effect is minimal. For the intermediate case, where the lifetime is on the order of tens to hundreds of nanoseconds, the excitation function retains some of its underlying shape but the peak tends to be shifted down in neutron energy (the convolution of the original excitation function with an exponential decay). It also offers the possibility of a lifetime measurement by fitting the decay curves corresponding to event times that are below the reaction threshold. A second scenario is that where the isomeric feeding accounts for a small fraction of the total intensity. In this case, the effects of isomers are a small perturbation and, as such, do not hamper the comparison of the experimental data with the calculated cross sections. The $\frac{13}{2}^+ \rightarrow \frac{9}{2}^+$ transition, the strongest γ-ray associated with the $(n,2n)$ channel, is fed weakly by known isomeric transitions. This feeding accounts for the appearance of cross section below the reaction threshold; however, the main shape of the excitation function, as well as the magnitude, is reproduced by the calculation. At the peak, which occurs at approximately 20 MeV neutron energy, the observed cross section for the $\frac{13}{2}^+ \rightarrow \frac{9}{2}^+$ transition is 0.195(10) b, while the calculated cross section is 0.14 b. The $\frac{17}{2}^+ \rightarrow \frac{13}{2}^+$ transition is fed strongly by isomeric transitions [with half lives of 47(1) and 38(4) ns] and demonstrates clearly the effect isomers can have on the apparent shape of the excitation functions. The remaining transitions do not suffer from the presence of isomers and show excellent agreement for the shapes of the excitation functions. Their magnitudes are larger than predicted, however. The 1605-keV transition is an example of ambiguity in the level scheme. Since the spin of the 1605.3-keV level is uncertain, an $I^\pi = \frac{7}{2}^-$ value was chosen for the purposes of the calculation; a different choice of spin would affect slightly the resulting magnitude calculated.

3. $^{92}Mo(n,3-5n\gamma)^{90-88}Mo$

The excitation functions for the lighter Mo nuclei, shown in Fig. 5, display overall very good agreement with the GNASH calculations, both in shape and magnitude. For ^{89}Mo and ^{88}Mo, the cross sections do not fall as rapidly as the calculations suggest; above 100 MeV neutron energy, they may be as much as a factor of 2 larger than predicted. However, it is satisfying that the portion of the excitation function dominated by the compound processes are very well reproduced.

B. The Nb isotopes

The Nb isotopes from ^{92}Nb, via the (n,p) channel, to ^{88}Nb, via the $(n,p4n)$ channel, were observed to be strongly populated in the reactions. The Nb isotopes offer interesting information due to the presence of many isomers, and a number of transitions were observed to populate the isomeric states and the ground states.

1. $^{92}Mo(n,p\gamma)^{92}Nb$

As shown in Fig. 6, several γ rays originating from ^{92}Nb were observed over two orders of magnitude variation in their intensity from a neutron energy of 2–3 MeV up to $E_n = 250$ MeV. The excitation functions for these lines show

the typical behavior characteristic of a charged-particle-exit channel; the compound portion of the excitation functions is very broad with a much slower rise in the cross section than a neutron exit channel. This is due to the Coulomb barrier for the evaporation of charged particles; for particle energies below the barrier tunneling is required and hence these processes are strongly hindered. While the (n,p) Q value is 0.426 MeV, most of the ^{92}Nb γ rays are not observed until $E_n \approx 2.5$ MeV, indicating that approximately 3 MeV of excitation energy is required before protons can be evaporated. The excitation function curves for both the 150-keV and 357-keV transitions suffer from unresolved doublets from other reaction channels with thresholds near $E_n = 15$ MeV, hence the ''humps'' observed in their excitation functions centered between $E_n = 20$ to 30 MeV are not attributed to the (n,p) channel. While the initial threshold behavior is well described, the peak magnitudes are larger than predicted, the most serious being the 164-keV $3_1^- \rightarrow 2_1^-$ transition by a factor of ≈ 2.5.

2. $^{92}Mo(n,pn\gamma)^{91}Nb$

^{91}Nb is the heaviest Nb isotope where composite particles could be emitted from the compound system. The difference in the thresholds between the (n,d) and (n,pn) reactions is 2.25 MeV. Shown in Fig. 7 are results for transitions originating from ^{91}Nb. Since none of the prompt γ rays are observed below the (n,pn) threshold of 7.54 MeV, there is no positive evidence of deuteron emission at low neutron bombarding energies. The first panel, which shows the excitation function for the 1082-keV γ ray has contributions from both the $\frac{5}{2}^- \rightarrow \frac{1}{2}^-$ ^{91}Nb transition and the $4_1^+ \rightarrow 2_1^+$ transition in ^{88}Zr. This latter contribution accounts for the ''background'' below the reaction threshold due to the presence of the 1.3-μs isomer in ^{88}Zr, as well as the structure observed above ≈ 20 MeV. However, below 18 MeV the shape (and essentially the magnitude) of the excitation function is due solely to the $\frac{5}{2}^- \rightarrow \frac{1}{2}^-$ transition in ^{91}Nb.

It is readily apparent upon inspection of Fig. 7 that there is very good agreement for the positive-parity states, but poorer agreement for the negative-parity states. The disagreement for the negative-parity states appears to increase with spin; the overprediction for the $\frac{13}{2}^- \rightarrow \frac{9}{2}^+$ transition is far greater than for the $\frac{9}{2}^- \rightarrow \frac{9}{2}^+$ transition. The low-spin transitions that feed the $\frac{1}{2}^-$ isomer, on the other hand, are larger than predicted. Since the channel cross section for ^{91}Nb is reproduced well (see Fig. 2), this points to a deficiency in the γ-ray cascade for this particular nucleus. It is unknown whether this effect is due to poor knowledge of the level scheme, e.g., no feeding from higher-lying levels because of nuclear structure, or reflects a parity dependence in the level density or γ-ray strength functions.

3. $^{92}Mo(n,p2n\gamma)^{90}Nb$

Four transitions in the odd-odd nucleus ^{90}Nb were resolved from other γ-ray transitions up to high neutron energy, and the excitation functions for these are shown in Fig. 8. The calculations are in good agreement with the data except for the $5_1^- \rightarrow 4_1^-$ transition. Interestingly, the poorest agreement occurs for the negative-parity state, as was observed in ^{91}Nb, but there is no explanation for this effect.

4. $^{92}Mo(n,p3n\gamma)^{89}Nb$ and $^{92}Mo(n,p4n\gamma)^{88}Nb$

Excitation functions for transitions from the lightest Nb nuclei observed in the present work, ^{89}Nb and ^{88}Nb, are shown in Fig. 9. Of interest are the threshold behaviors of the excitation functions in that they increase more slowly than the calculations predict. As well, using the empirical value determined from the ^{92}Nb data that the γ rays are not observed until ≈ 3 MeV above threshold, ^{89}Nb γ rays would not be expected below ≈ 33 MeV. However, the 932 keV $\frac{17}{2}^+ \rightarrow \frac{13}{2}^+$ transition is observed at 28 MeV; this is likely a result of feeding from known isomeric states (2151-keV level with $t_{1/2} = 6$ ns and 2193-keV level with $t_{1/2} = 14$ ns). For ^{88}Nb, the calculated excitation function is much narrower then the observed one.

C. The Zr isotopes

Excitation functions for γ rays from the Zr isotopes, ranging from ^{91}Zr to ^{86}Zr, are shown in Figs. 10–13. In general, the calculations are in good agreement with the experimental excitations functions, especially the shape of the curves.

1. $^{92}Mo(n,2p\gamma)^{91}Zr$ and $^{92}Mo(n,2pn\gamma)^{90}Zr$

The heaviest Zr isotope that can be observed is ^{91}Zr via the $(n,2p)$ channel. The excitation functions for two γ-rays from ^{91}Zr are shown in Fig. 10. Unfortunately, the ^{91}Zr $\frac{9}{2}^+ \rightarrow \frac{5}{2}^+$ ground-state transition is not resolved from a ^{89}Zr transition. The ^{91}Zr 2170-keV $\frac{11}{2}^- \rightarrow \frac{5}{2}^+$ ground-state transition is in excellent agreement with the calculations.

The lower panels of Fig. 10 show the excitation functions for transitions belonging to ^{90}Zr. The $(n,2pn)$ threshold is 12.75 MeV and, since there is no observable intensity below this energy, there is no evidence for composite particles like ^{3}He, which has a threshold of 4.95 MeV, being emitted. The agreement between the experimental data and the calculations for the shape of the excitation functions is reasonable, although the experimental excitation functions peak at 30 MeV rather than at 35 MeV as predicted by the calculation. The calculations do predict larger cross sections than observed, by a factor of about 2.5 over most of the range of neutron energies.

2. ^{92}Mo$(n,\alpha/2p2n\gamma)^{89}$Zr

Shown in Fig. 11 are excitation functions for transitions assigned to ^{89}Zr. The curves show a definite double-humped structure, which is attributed to α emission at low neutron energies followed by contributions from $2p2n$ emission for higher neutron energies. The threshold for the ^{92}Mo(n,α) reaction is 0 MeV, whereas that for the ^{92}Mo$(n,2p2n)$ reaction is 24.86 MeV. The actual threshold for the emission of an α particle is higher than the kinematic threshold due to the Coulomb barrier; the apparent threshold is about 10 MeV. In the first panel, the 1943-keV $\frac{13}{2}^+ \rightarrow \frac{9}{2}^+$ ground-state transition has a tail extending down to approximately 5 MeV neutron energy. This tail is attributed to weak feeding from

known isomeric states with half-lives in the range of several-to-dozens of nanoseconds. However, the basic shape of the excitation function is unaffected by the weakly populated isomeric states. The 178-keV $\frac{13}{2}^- \rightarrow \frac{13}{2}^+$ transition does not appear to suffer from the isomeric feeding problem. These transitions indicate that the α-particle emission is a rather weak process; the peak cross section occurs at $E_n \simeq 18$ MeV and is about a factor of 4 lower than the peak cross section for the $2p2n$ channel that occurs at $E_n = 50$ MeV. The 2121-keV $\frac{13}{2}^- \rightarrow \frac{9}{2}^+$ ground state transition is contaminated at low neutron energies by a ^{91}Nb line, making the appearance of the ''α hump'' more pronounced, but it is thought to contribute less than 10% at higher neutron energies. The 769-keV $\frac{19}{2} \rightarrow \frac{17}{2}$ transition (note that the parities are unknown for these levels) could not be followed to low neutron energies due to weak statistics for this peak. This may indicate that the α-particle emission is suppressed relative to the $(n,2p2n)$ channel for higher angular momentum states. As can be seen in Fig. 11, the GNASH calculations using the default level density parameters (solid lines) underestimate the α-particle emission below the $2p2n$ threshold, the calculated magnitudes are a factor of 2–3 smaller than observed. Above the $2p2n$ threshold, the calculations reproduce well both the shape and the magnitude of the cross sections, except for the 769-keV transition. The adjustment of the level density parameters (dashed lines) improves the prediction of the (n,α) channel, but at the expense of the good description of the $(n,2p2n)$ channel.

3. $^{92}Mo(n,\alpha n/2p3n\gamma)^{88}Zr$

Figure 12 shows results for transitions from ^{88}Zr. The $2_1^+ \rightarrow 0_1^+$, $5_1^- \rightarrow 4_1^+$, and $6_1^+ \rightarrow 4_1^+$ transitions show the effects of the 1.3-μs 8^+ isomer, which causes a background that is evident below $E_n = 10$ MeV. This effect is especially clear with the $6_1^+ \rightarrow 4_1^+$ transition which is directly fed from the 8^+ isomer, and in this case the magnitude of the excitation function is affected significantly. The shapes of the excitation functions are reproduced by the calculations, although the αn-exit channel peaks at lower energies than calculated. Above the $2p3n$ threshold ($E_t = 34$ MeV), the excitation functions are broader and have a less pronounced peak than the calculations predict. The peak in the $(n,\alpha n)$ channel cross section is approximately a factor of 2 smaller than the peak in the $(n,2p3n)$ channel cross section, whereas for ^{89}Zr the corresponding peak cross section ratio was a factor of 4.

4. $^{92}Mo(n,\alpha 2n/2p4n\gamma)^{87}Zr$ and $^{92}Mo(n,\alpha 3n/2p5n\gamma)^{86}Zr$

Figure 13 displays the excitations functions observed for transitions assigned to ^{87}Zr and ^{86}Zr. It is interesting to note that the cross sections still have an observable dip between the $(n,\alpha xn)$ and $[n,2p(x+2)n]$ channels. While the magnitudes of the cross sections for the transitions in ^{87}Zr are reproduced well, those for ^{86}Zr are much smaller than calculated; the 752-keV $2_1^+ \rightarrow 0_{\text{g.s.}}^+$ transition in ^{86}Zr is calculated to have a peak cross section of 80 mb at $E_n = 100$ MeV, whereas experimentally the peak cross section observed is 32.5(15) mb at $E_n = 120$ MeV.

In the $\gamma\gamma$ coincidence spectra, the low-lying portion of the yrast band for ^{84}Zr [from the $(n,\alpha 5n/2p7n)$ channel] was observed very weakly. However, no resolved ^{84}Zr transitions could be located in the singles spectra, and the others members of the doublets were the dominating ones so that the shape of the excitation functions for ^{84}Zr were not obtained.

D. The Y isotopes

The $(n,\alpha pxn)$ and $[n,3p(x+2)n]$ channels lead to the odd-A and odd-odd Y isotopes. These particular channels were difficult to observe due to the highly fragmented γ-ray cascade in the low-lying portions of their level schemes. The strongest resolved transitions observed from ^{88}Y, ^{86}Y, ^{85}Y, and ^{84}Y are displayed in Fig. 14. While one expects that ^{87}Y is produced with comparable yield, no resolved transition from ^{87}Y could be positively identified.

The thresholds for the $(n,3pxn)$ channels are 32.8, 54.2, 63.8, and 75.7 MeV for ^{88}Y, ^{86}Y, ^{85}Y, and ^{84}Y, respectively. For all the transitions displayed in Fig. 14, there appears observable cross section below these thresholds. These yields may be attributed to $(n,\alpha pxn)$ channels, which have thresholds of 4.2, 25.6, 35.2, and 47.1 MeV, respectively. However, some of the transitions appear immediately above their Q-value thresholds, which is unexpected given that both the α particle and the proton must tunnel through the Coulomb barrier. In the Zr isotopes, for example, it was found that a neutron bombarding energy approximately 10 MeV above threshold was needed for the Zr γ rays to be observed. This suggests that some of the Y γ-ray yields may have contributions from other unresolved γ rays with lower thresholds.

E. The Sr isotopes

The Sr isotopes represent more complex particle-emission channels, and one might expect combinations of $2\alpha xn$, $\alpha 2pxn$, and $4pxn$ processes to be evident. The most obvious isotope in which to look for these processes is ^{84}Sr since the $2_1^+ \rightarrow 0_{\text{g.s.}}^+$ transition carries essentially all of the formation cross section for ^{84}Sr, unlike, e.g., the situation in ^{85}Sr. The $(n,2\alpha n)$ threshold is 11.1 MeV, and using the empirical value that α-particle emission becomes observed $\simeq 10$ MeV above threshold, as was found for ^{88}Zr, it can be estimated that ^{84}Sr should be observable around $E_n = 30$ MeV (10 MeV for each α particle). An examination of the excitation functions in Fig. 15 shows that for ^{84}Sr this empirical estimate is fulfilled. The observed threshold for ^{84}Sr does indeed appear at $E_n = 30$ MeV, well below the $(n,\alpha 2p3n)$ threshold of 39.7 MeV. A local maximum of 3.7(4) mb in the cross section is reached at $E_n = 47$ MeV, above the $(n,\alpha 2p3n)$ threshold but below the $(n,4p5n)$ threshold of 68.3 MeV. At the $(n,4p5n)$ threshold, the cross section increases again reaching a maximum of 22.3(10) mb at $E_n = 120$ MeV. The GNASH calculations greatly underestimates the $(n,2\alpha n)$ channel contribution below $E_n = 60$ MeV, but is in good overall agreement above $E_n = 80$ MeV.

The main production mechanisms of ^{86}Sr are expected to be via the $(n,\alpha 2pn)$ and $(n,4p3n)$ channels, with thresholds of 19.5 and 48.1 MeV, respectively. The excitation function for the $2_1^+ \rightarrow 0_{\text{g.s.}}^+$ transition in ^{86}Sr shown in Fig. 15 indicates that the observable threshold is at approximately $E_n = 40$ MeV, reaching a local maximum at about $E_n = 64$ MeV, and then rising again at $E_n = 90$ MeV attaining a relatively constant value up to $E_n = 250$ MeV. The GNASH calculations reproduce very well the behavior up to $E_n = 100$ MeV after which the calculation and the data begin to diverge.

The remaining Sr isotopes observed, ^{85}Sr, ^{83}Sr, ^{82}Sr, and ^{80}Sr do not show the same kind of structure in their excitation functions although for high neutron bombarding energies the finite time resolution may smear the effects. All of these channels appear, however, below or at the thresholds for the $(n,4pxn)$ reactions, which are at 59.7, 80.4, 89.4, and 111.5 MeV, respectively, indicating contributions from the $(n,\alpha 2pxn)$ reactions (with thresholds at 31.1, 51.8, 60.7, and 73.4 MeV, respectively). The excitation functions is some cases have differences as large as an order of magnitude compared with the GNASH results.

F. Isomeric state population

In a number of nuclei, γ-ray transitions populating both the ground state and isomeric states within the same nucleus were observed. The population of isomeric states in neutron-induced reactions has long been of interest. These cross sections are a sensitive probe of the reaction modeling, since typically the very existence of isomeric states is due to a very large spin difference compared to the ground state and their population allows one to probe the consequences of the γ-ray cascade and the entry region distribution. The populations of isomeric states also have a number of practical applications, such as in neutron dosimetry where the isomer-to-ground state populations can be used as probes of the neutron spectra that induced the transitions.

Shown in Fig. 16 are the ratios for specific γ rays populating the isomer and the ground state for ^{92,91,90}Nb and ^{90}Zr. These are not the only isomeric states observed to be populated, but only these particular cases involve isomeric states with long lifetimes where their population could be followed up to high neutron energy ($E_n > 10$ MeV). Also shown are the GNASH calculations for the corresponding γ-ray ratio. For ^{92}Nb, the ratio of the ground state to isomeric state population for the 2^- isomer ($t_{1/2} = 5.9$ μs) and the 2^+ isomer ($t_{1/2} = 10.15$ d) is in good agreement with the GNASH calculation up to approximately $E_n = 10$ MeV. Above this energy, the experimental ratio falls below the predicted curve. For the population of the 2^+ isomer, the data could be extracted up to $E_n = 14$ MeV only, since the transitions were part of unresolved doublets above this energy. The population of the 2^- isomer shows clearly the decreasing population of the ground state relative to the low-spin isomeric state at high neutron energies. In ^{91}Nb, the ratio of the population of the 60.9-d $\frac{1}{2}^-$ isomer to that of the ground state is reproduced well by the calculation up to $E_n = 30$ MeV, at which point the ratio increases significantly above the calculation. A similar effect is observed in ^{90}Nb, above $E_n = 50$ MeV for the 63-μs 6^+ isomer and above $E_n = 25$ MeV for the 18.8-s 4^- isomer. In ^{90}Zr, the 809-ms 5^- isomer to ground state population is reproduced well until approximately $E_n = 100$ MeV.

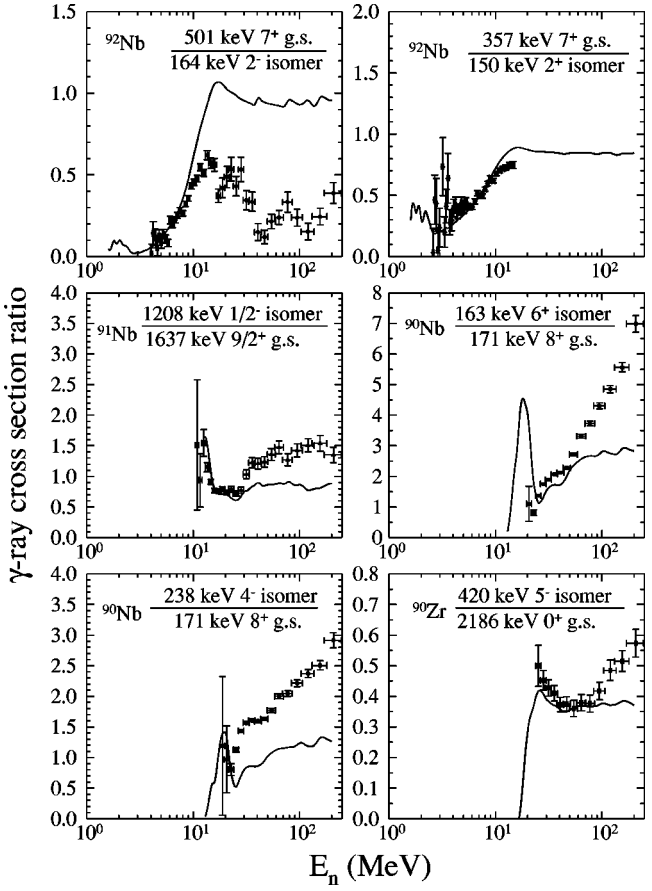

FIG. 16. Ratio of γ-ray cross section indicated for the population of isomers and ground states in ^{92,91,90}Nb and ^{90}Zr. The labels give the energies of the γ rays feeding the particular levels listed. The ratios of cross sections are free of any normalizations, either to the overall scale set by the 1509-keV $2^+ \rightarrow 0^+$ transition in ^{92}Mo or to the neutron flux.

For all the cases discussed in this section, it must be remembered that these are not the *channel* cross section ratios but rather the partial γ-ray cross section ratios. As such, the GNASH calculations can suffer from the same kinds of problems of incomplete knowledge of level schemes, etc., as was discussed in the previous sections. The fact that the ratios appear to be much more poorly reproduced in ^{92}Nb and ^{90}Nb may be related to this lack of knowledge since these nuclei are less well known than their odd-*A* or even-even neighbors. Also, the fact that the data and the calculations tend to diverge with increasing neutron energies may imply problems with the description of the spin distribution in preequilibrium processes.

V. SUMMARY

An experiment was performed at the LANSCE-WNR spallation neutron source using the GEANIE γ-ray spec-

trometer and a scattering sample of ^{92}Mo. Excitation functions, normalized at one point to the calculated $2_1^+ \rightarrow 0_{\text{g.s.}}^+$ transition in ^{92}Mo, were extracted for a total of 26 different isotopes for neutron energies up to 250 MeV. The lightest isotope observed was ^{80}Sr from the $(n,\alpha 2p7n$ or $4p9n)$ reaction. The present experimental data, which is one of the most extensive data sets ever collected for fast neutron-induced reactions, are compared with the results of GNASH calculations for the partial γ-ray cross sections. The enhanced Hauser-Feshbach calculations include compound nucleus, preequilibrium, multiple-preequilibrium, and direct reaction processes.

The GNASH calculations reproduce reasonably well the shapes and magnitudes in the excitations functions of the reaction γ rays observed. Problems arise, however, if there is insufficient knowledge in the level scheme, i.e., in the placements of transitions and levels. Further problems may arise in the description of the γ-ray cascade. This may be partially responsible for the effects observed in ^{91}Nb, where transitions from positive-parity states are reproduced well by the calculations and those from negative-parity states are not. Composite-particle emission, the most important of which are α particles, also appears to be a source of discrepancy between the model calculations and the data. At low neutron energies (below 30 MeV), the α-particle emission cross sections are larger than predicted. For higher-multiplicity charged-particle exit channels, the calculations often predict greater cross sections than observed. Complex-particle emission in high-energy reactions is an area that clearly needs much attention experimentally and theoretically.

ACKNOWLEDGMENTS

This work was performed under the auspices of the U.S. Department of Energy by Lawrence Livermore National Laboratory and Los Alamos National Laboratory under Contract Nos. W-7405-ENG-48 and W-7405-ENG-36. Support for S.W.Y. was provided by the U.S. National Science Foundation under Grant No. PHY-9803784, and for E.T. by DOE Grant No. DE-FG02-97-ER41042.

[1] J. A. Becker and R. O. Nelson, Nucl. Phys. News **7**, 11 (1997).
[2] L. A. Bernstein, J. A. Becker, W. Younes, D. E. Archer, K. Hauschild, G. D. Johns, R. O. Nelson, W. S. Wilburn, and D. M. Drake, Phys. Rev. C **57**, R2799 (1998).
[3] P. G. Young, E. D. Arthur, and M. B. Chadwick, Los Alamos National Laboratory Report No. LA-UR-96-3739.
[4] A. Pavlik, H. Hitzenberger-Schauer, H. Vonach, M. B. Chadwick, R. C. Haight, R. O. Nelson, and P. G. Young, Phys. Rev. C **57**, 2416 (1998).
[5] S. A. Wender, S. Balestrini, A. Brown, R. C. Haight, C. M. Laymon, T. M. Lee, P. W. Lisowski, W. McCorkle, R. O. Nelson, W. Parker, and N. W. Hill, Nucl. Instrum. Methods Phys. Res. A **336**, 226 (1993).
[6] D. C. Radford, RADWARE analysis package as maintained at radware.phy.ornl.gov.
[7] P. W. Lisowski, A. Gavron, W. E. Parker, J. L. Ullmann, S. J. Balestrini, A. D. Carlson, O. A. Wasson, and N. W. Hill, ''Fission cross sections in the intermediate energy range,'' Proceedings of the Specialists' Meeting on Neutron Cross Section Standards Above 20 MeV, Uppsala, Sweden, 1991, Nuclear Energy Agency Nuclear Data Committee Report No. NEANDC-305 '*U*', Paris, 1991, p. 177.
[8] J. Raynal, ''Notes on ECIS94'' Commissariat à l'Energie Atomique CEA, Saclay, France, 1994, CEA-N-2772, p. 1.
[9] D. Wilmore and P. E. Hodgson, Nucl. Phys. **55**, 673 (1964).
[10] D. G. Madland, ''Recent results in the development of a global medium-energy nucleon-nucleus optical-model potential,'' in Proceedings of the Specialists' Meeting on Preequilibrium Nuclear Reactions, Semmering, Austria, 1988, edited by B. Strohmaier, Nuclear Energy Agency Nuclear Data Committee Report No. NEANDC-245 '*U*', Paris, 1988, p. 103.
[11] C. M. Perey and F. G. Perey, At. Data Nucl. Data Tables **17**, 1 (1976).
[12] J. Lohr and W. Haeberli, Nucl. Phys. **A232**, 381 (1974).
[13] F. D. Becchetti, Jr. and G. W. Greenlees, in *Polarization Phenomena in Nuclear Reactions*, edited by H. H. Barschall and W. Haeberli (University of Wisconsin Press, Madison, 1971), p. 682.
[14] L. McFadden and G. R. Satchler, Nucl. Phys. **84**, 177 (1966).
[15] J. Kopecky and M. Uhl, Phys. Rev. C **41**, 1941 (1990).
[16] C. Kalbach, Z. Phys. A **382**, 401 (1977).
[17] C. Kalbach, Centre d-Etudes Nucléaires de Saclay Rapport Interne, DPh-N/BE/74/3, 1974.
[18] M. B. Chadwick, P. G. Young, D. C. George, and Y. Watanabe, Phys. Rev. C **50**, 996 (1994).
[19] *Handbook for Calculations of nuclear reaction data: Reference input parameter library* (International Atomic Energy Agency, Vienna, Austria, 1998), IAEA-TECDOC-1034.
[20] Data as compiled at the National Nuclear Data Center, Brookhaven National Laboratory.
[21] P. E. Garrett, L. A. Bernstein, J. A. Becker, K. Hauschild, C. A. McGrath, D. P. McNabb, W. Younes, E. Tavukcu, G. D. Johns, R. O. Nelson, W. S. Wilburn, and S. W. Yates, Phys. Rev. C **62**, 014307 (2000).
[22] A. V. Ignatyuk, G. N. Smirenkin, and A. S. Tishin, Yad. Fiz. **21**, 485 (1975) [Sov. J. Nucl. Phys. **21**, 255 (1975)].